RSC Advances

PAPER

View Article Online
View Journal | View Issue

Cite this: RSC Adv., 2014, 4, 64187

Electrodeposition of manganese dioxide film on activated carbon paper and its application in supercapacitors with high rate capability

Yongfu Qiu,[a] Pingru Xu,[a] Bing Guo,[a] Zhiyu Cheng,*[a] Hongbo Fan,[a] Minlin Yang,[a] Xiaoxi Yang[a] and Jianhui Li[b]

Received 26th September 2014
Accepted 11th November 2014

DOI: 10.1039/c4ra11127c

www.rsc.org/advances

In this research magnesium dioxide (MnO_2) is electrodeposited over activated carbon paper (ACP) to form a composited MnO_2/ACP material. The as-prepared MnO_2/ACP shows excellent capacitance performance with a high specific capacitance of 485.4 F g^{-1} calculated from a discharge curve with current density 2.0 A g^{-1}, owing to its enlarged specific surface area and improved electronic conductivity. Moreover, the MnO_2/ACP possesses remarkable rate capability due to the easy access of electrolytic ions, leading to complete utilization of MnO_2 active material for supercapacitors. To summarize, the electrodeposition of MnO_2 thin film on activated carbon paper is reported for the first time, and the composited MnO_2/ACP is a promising electrode material for building up efficient supercapacitors.

1. Introduction

Supercapacitors as energy storage devices have attracted significant attention over the past few years due to their fast charge–discharge rates, high power densities, long lifetimes and a good safety record.[1–7] Generally, supercapacitors are classified into electrical double layer capacitors (EDLCs)[1,2] and pseudocapacitors[3–7] on the basis of the different charge storage mechanisms. Compared to EDLCs, pseudocapacitors, which are based on metal oxides or conducting polymers are more attractive because of their higher capacitance and energy density through faradic reactions.[3–7] Among various pseudocapacitive materials, manganese dioxide (MnO_2) has been considered as the most attractive candidate in terms of its superior capacitor performance (the theoretical capacitance 1370 F g^{-1}), environmentally friendly and cost-effective.[8] However, supercapacitors based on MnO_2 alone often show poor rate capability owing to its low electrical conductivity (10^{-5} to 10^{-6} S cm^{-1}).[9,10] To date, a lot of efforts have been devoted to grow MnO_2 nanostructures on stable carbon substrates, such as graphite, carbon nanotube, reduced graphene oxide, graphene and carbon nano-onions, because of their high electrical conductivity and good mechanical strength, in order to maximize the utilization of MnO_2 pseudocapacity.[11–15]

Herein, carbon papers are used as substrates or current collectors for MnO_2 based pseudocapacitors due to their chemical stability in strong acidic solution, highly electrical conductivity and cost-effectiveness.[16] However, commercial carbon paper is hydrophobic and generally has low specific surface area, thus appropriate surface chemical modification is required to ensure their wettability and electrochemical activity before they can be used as substrates.[17–19] Electrodeposition technique is considered as an effective route to prepare manganese oxide film on substrates.[15] In this research, the electrodeposited MnO_2 thin film on activated carbon paper (MnO_2/ACP) possesses a specific capacitance as high as 485.4 F g^{-1} calculated from discharge curve with current density 2.0 A g^{-1}. The corresponding values of MnO_2/ACP calculated from cyclic voltammograms at scan rates of 20 and 50 mV s^{-1} are 312.0 and 235.2 F g^{-1}, respectively, which retain 81.7% and 61.6% of the corresponding value at 10 mV s^{-1} (382.0 F g^{-1}). This indicates that the sample MnO_2/ACP possesses good rate capability as an active electrode material for supercapacitors.

2. Experimental

2.1 Preparation of activated carbon paper (ACP)

The commercial carbon papers (CP, purchased from Jixing Sheng An Corp., 1.0 cm × 4.0 cm, the thickness 0.30 mm, mass density 32 mg cm^{-2}) were soaked in a solution mixture containing 20 mL of concentrated H_2SO_4 (98%) and 2 g of $KMnO_4$ (slowly added into H_2SO_4) at 25 °C for 120 s. Afterwards, the activated carbon papers were heated at 150 °C for 2 h, and then washed three times with distilled water. This treatment is denoted as a modified Hummer's method[20] and the activated carbon paper was abbreviated as ACP.

[a]College of Chemistry and Environmental Engineering, Guangdong Provincial Key Laboratory of Distributed Energy Systems, Dongguan University of Technology, Guangdong 523808, P. R. China. E-mail: mszycheng@scut.edu.cn; qiuyf1979@foxmail.com; Fax: +86 769 2286 1232; Tel: +86 769 2286 1232

[b]National Engineering Laboratory for Green Chemical Productions of Alcohols–Ethers–Esters, College of Chemistry and Chemical Engineering, Xiamen University, 361005, Xiamen, China

2.2 Preparation of MnO_2/activated carbon paper (MnO_2/ACP)

The MnO_2 film was formed on activated carbon paper by anodic electrochemical deposition in a solution of 0.1 M manganese acetate at 25 °C for 120 s (0.90 V *vs.* Ag/AgCl). Consequently, the as-deposited MnO_2 film on the activated carbon paper was annealed at 150 °C for 2.0 h and denoted as MnO_2/ACP. For comparison, MnO_2 film was deposited on commercial carbon paper and denoted as MnO_2/CP.

2.3 Characterization

The morphologies and elemental microprobe analyses were performed on a JEOL 6701F scanning electron microscope (SEM) equipped with an INCA PentaFETx3 (Oxford Instruments) energy dispersive X-ray spectroscopy (EDS) detector. Atomic force microscope (AFM) images were obtained on a scanning probe microscope (CSPM5600, Being Nano-Instruments Ltd.). The specific surface areas of the samples were determined by nitrogen adsorption at 77 K with a JWGB SCI. & TECH BK132F automatic adsorption apparatus; contact angles were observed using a surface tension meter (Dataphysics OCA20, Germany) at 25 °C.

Cyclic voltammetry (CV) and galvanostatic charge–discharge measurements were performed in a three-electrode system using a CHI 440a electrochemical work station, with 1.0 M Na_2SO_4 as the electrolyte solution. As-prepared samples with an area of 1.0 cm^2 were used as the working electrode, Ag/AgCl (3.0 M KCl) and a Pt wire as the reference and counter electrodes, respectively. Electrochemical impedance spectroscopy (EIS) measurements were carried out using a potentiostat (EG & G, M2273), the frequency range analyzed was 0.1 Hz to 100 Hz with AC amplitude of 10 mV.

2.4 Calculation

The specific capacitance of the electrode can be calculated using the following equation:[21]

$$C = \frac{1}{mv(U_c - U_a)} \int_{U_a}^{U_c} I(U)\mathrm{d}U$$

where C is the specific capacitance (F g^{-1}), m is mass of electroactive material (g), v is the potential scan rate (V s^{-1}), $U_c - U_a$ is the sweep potential range of the discharging branch and $I(U)$ denotes the response current density (A g^{-1}). Alternatively, gravimetric capacitance for a single electrode was calculated from the discharge curve in a three-electrode cell as $C_{single} = \frac{I\Delta t}{\Delta V}$, where I is the constant current (A g^{-1}), Δt is the discharge time, ΔV is the voltage change during the discharge process.[21]

3. Results and discussion

3.1 SEM, EDS and AFM

Fig. 1A and B are the SEM images of the surface morphologies of CP and ACP. In contrast with that of CP, the surface of ACP is rough, indicating that it underwent a change due to the modified Hummers treatment. SEM images of MnO_2/CP and MnO_2/ACP are shown in Fig. 1C and D. It was observed that layers of MnO_2film covered the surfaces of CP and ACP after deposition. Obviously, there were more cracks on the surface of MnO_2/ACP compared to that of MnO_2/CP. In order to detect the composition of the film, EDS profile was collected and shown in Fig. 1E. It was clearly revealed that the film is composed of Mn and O with a ratio of about 1 : 2, which is consistent with the chemical formula of MnO_2. AFM results in Fig. 1F shows that the thickness of the MnO_2 film are about 0.58–1.25 μm. The mass loadings of MnO_2 for MnO_2/CP and MnO_2/ACP are 0.48 and 0.51 mg cm^{-2}.

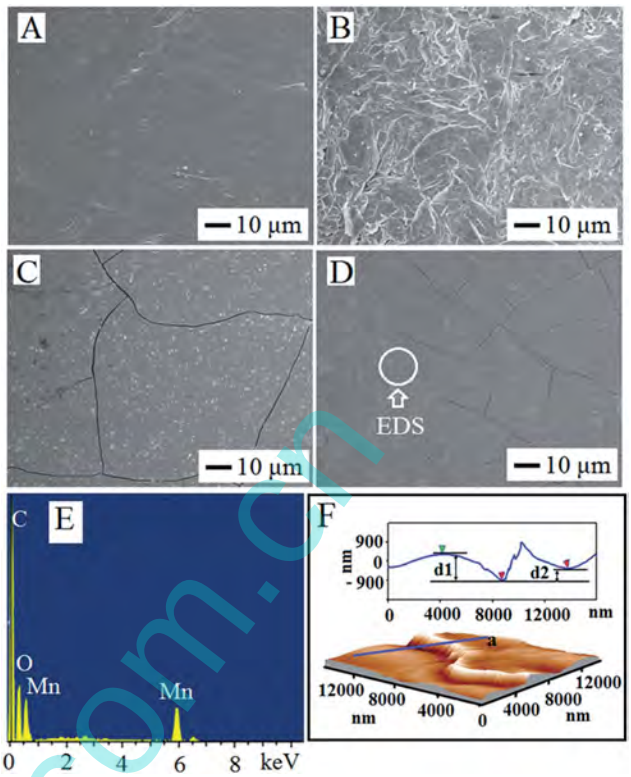

Fig. 1 SEM images of: (A) CP; (B) ACP; (C)MnO_2/CP; (D)MnO_2/ACP; (E) EDS profile of the MnO_2 film of the area marked by circle in (D); and (F) AFM image of MnO_2/ACP (down), and inset is the profile of the topography with scan line a.

3.2 N_2 adsorption–desorption and XRD

As shown in Fig. 2A, nitrogen adsorption–desorption measurements were performed to examine surface properties of the samples. The sharp increase in the N_2 adsorbed quantity near the relative pressure P/P_o of 1 indicates that only macropores exist in the samples of ACP and MnO_2/ACP. According to the Brunnauer–Emmett–Teller (BET) analysis, the specific surface areas for ACP and MnO_2/ACP are 21.1 and 7.7 m^2 g^{-1}. The specific surface area for MnO_2/ACP is lower compared to ACP because the rough surface was covered by a thin layer of MnO_2.

The crystalline structures of ACP and MnO_2/ACP were characterized by powder X-ray diffraction (XRD) and the results are shown in Fig. 2B. The XRD pattern for ACP in Fig. 2B is

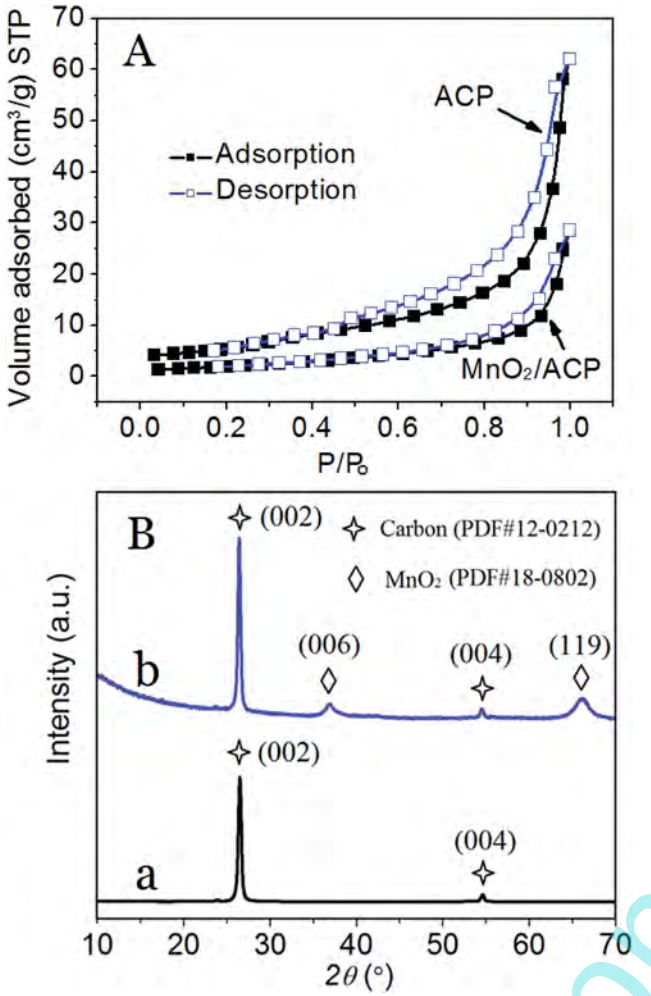

Fig. 2 (A) N_2 adsorption–desorption isotherms; (B) XRD patterns of (a) ACP; (b) MnO_2/ACP.

attributed to carbon (PDF#12-0212) with lattice constants of $a = 0.2464$ nm and $c = 0.6736$ nm. In addition to the two peaks at $2\theta = 26.4°$ and 54.5° for carbon, another two diffraction peaks at $2\theta = 36.8°$ and 65.7° indexed to MnO_2 birnessite structure (PDF#18-0802, lattice constants $a = 0.5820$ nm and $c = 0.1462$ nm) in pattern *b* were observed. The grain diameter of the MnO_2 on ACP can be calculated using Scherrer's equation,[22] $D = \frac{0.9\lambda}{\beta \cos \theta}$, where β is the broadening of diffraction line measured at half maximum intensity (radians) and $\lambda = 0.154056$ nm, the wavelength of the Cu K_α X-ray. The grain diameter of the MnO_2 in the film was calculated to be 6.8 nm.

3.3 Wetting property

The wetting property of the sample was characterized by the water contact angle test.[23] The contact angle is the angle measured through the liquid, at which a liquid–vapor interface meets a solid surface, which quantifies the wettability of a solid surface by a liquid *via* the Young equation:[23] $0 = \gamma_{SG} - \gamma_{SL} - \gamma_{LG} \cos \theta_C$, where γ_{SG} is the solid–vapor interfacial energy, γ_{SL} as the solid–liquid interfacial energy, γ_{LG} as the liquid–vapor interfacial energy and θ_C is the equilibrium contact angle. Generally, if the water contact angle is smaller than 90°, the solid surface is considered as hydrophilic. The contact angles of water droplets on the surface of CP, ACP, MnO_2/CP and MnO_2/ACP are shown in Fig. 3. Obviously, the contact angle $72.0 \pm 0.3°$ for ACP is smaller than that of CP $117.0 \pm 0.5°$, indicating that the surface hydrophilicity is enhanced over the modified Hummers treatment. This enhancement could be ascribed to the hydrophilic groups such as hydroxyl (–OH), carbonyl (>C=O) and carboxyl (–COOH) introduced onto the surface of carbon papers and they act as strong polar sites that absorb water molecules.[24] Further, the contact angles for MnO_2/CP and MnO_2/ACP are $49.5 \pm 0.5°$ and $42.0 \pm 0.5°$, both lower than those of their counterparts, suggesting that the intake of MnO_2 brings enhanced hydrophilicity to both CP and ACP.

3.4 Cyclic voltammetry and galvanostatic charge–discharge measurements

The electrochemical performance of as-prepared samples were investigated in a three-electrode system, in which 1.0 M Na_2SO_4 was used as electrolyte, as-prepared samples as working electrode, Ag/AgCl and Pt wire as the reference and counter electrodes.[25,26] The cyclic voltammograms collected at different scan rates for the samples are shown in Fig. 4. From Fig. 4A to D, it is obvious that the enclosing areas of the CV curves increase with the increasing potential scan rates and the specific capacitance could be calculated from CV curves using the following equation:[21] $C = \frac{1}{mv(U_c - U_a)} \int_{U_a}^{U_c} I(U)\mathrm{d}U$. The calculated specific capacitances of samples under 10 mV s^{-1} are shown in Fig. 4F. The corresponding values for CP and ACP are 113.0 and 158.6 F g^{-1}, while those for MnO_2/CP and MnO_2/ACP are 326.8 and 382.0 F g^{-1}, suggesting that the loading of MnO_2 thin films on

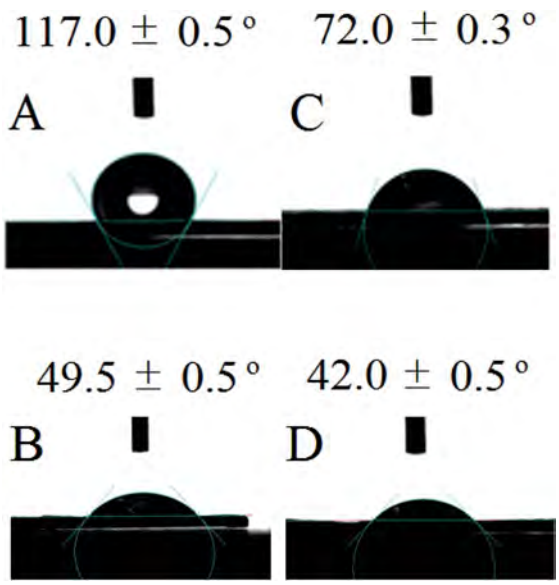

Fig. 3 Cross-sectional views of water droplets on (A) CP; (B) MnO_2/CP and (C) ACP; (D) MnO_2/ACP.

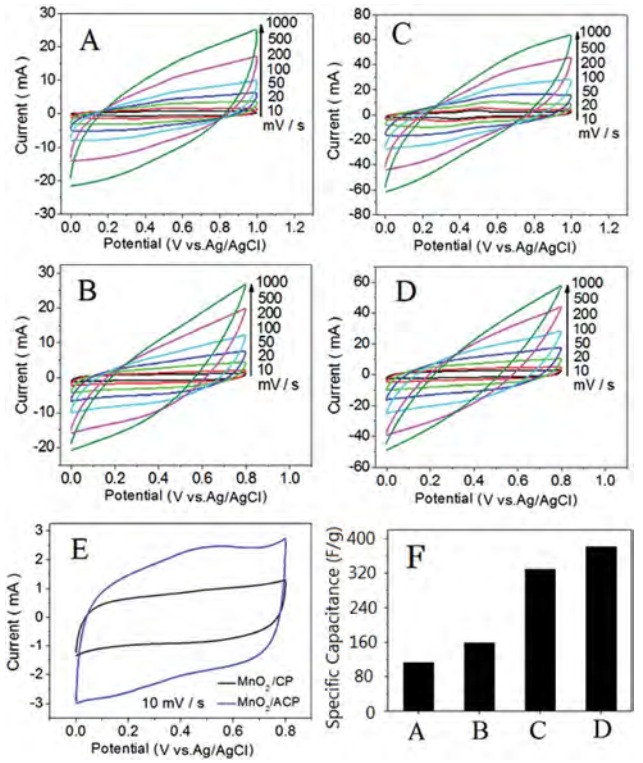

Fig. 4 Cyclic voltammograms collected at different scan rates for: (A) CP; (B) MnO_2/CP; (C) ACP and (D) MnO_2/ACP; (E) enlarged CV diagrams for MnO_2/CP and MnO_2/ACP at a scan rate of 10 mV s^{-1}; (F) calculated specific capacitances of the samples from a plot of A–D at a scan rate of 10 mV s^{-1}.

CP or ACP dramatically increases the specific capacitances. In Fig. 4E, the enlarged CV diagrams for MnO_2/CP and MnO_2/ACP show quasi-rectangular shapes as the typical signature of the ideal capacitive materials, exhibiting their good electrochemical behaviors. Furthermore, the specific capacitance of 382.0 F g^{-1} for MnO_2/ACP is higher than that for MnO_2/CP, which is 326.8 F g^{-1}, indicating that the activated surface of carbon paper has a remarkable effect on the electrochemical behavior of the composited electrodes, which is due to the enlarged specific surface area and the improved hydrophilicity.

The rate capabilities of electrode materials could also be seen in the CV curves at different scan rates shown in Fig. 4. These CV curves exhibit rectangular shapes at low scan rates (<100 mV s^{-1}), and they clearly deviate from rectangular shapes at increased scan rate (>100 mV s^{-1}). This could be explained by the relatively slow diffusion of Na^+ within the MnO_2 matrix[27,28] and accordingly the MnO_2 materials under the interface does not actively contribute to the performance of pseudocapacitance. The specific capacitances of MnO_2/ACP calculated from cyclic voltammograms at scan rates of 20 and 50 mV s^{-1} are 312.0 and 235.2 F g^{-1} respectively, which retain 81.7% and 61.6% of the corresponding value at 10 mV s^{-1} (382.0 F g^{-1}). This implies that the MnO_2/ACP sample possesses better rate capability as active electrode material for supercapacitors compared to others.

The MnO_2/ACP exhibits the best supercapacitor performance, as further confirmed by the galvanostatic charge–discharge measurements in a three-electrode system. Fig. 5A shows the charge–discharge curves for MnO_2/ACP at different current densities. These curves generally show symmetrical and linear profiles, indicating that MnO_2/ACP exhibits excellent supercapacitive behavior. The specific capacitances for a single electrode calculated from the discharge curve are shown in Fig. 5B.[21] When the current densities are 2.0, 4.0, 6.0, 8.0, 10.0 and 12.0 A g^{-1}, the corresponding specific capacitances of 485.4, 397.2, 336.8, 295.4, 265.0 and 237.8 F g^{-1} could be observed, which suggest that superior reversible redox reactions take place within MnO_2/ACP, leading to its excellent supercapacitive behavior. The specific capacitance for MnO_2/ACP is 295.4 F g^{-1} at current density 10 A g^{-1}, which is higher than 250.0 F g^{-1} for the flat MnO_2 electrode and lower than 714.1 F g^{-1} for three-dimensional Au/MnO_2 nanocone arrays electrode.[29]

Good capacitance retention is crucial for practical supercapacitors.[29] The capacitance retention test over 2000 cycles for MnO_2/ACP was performed at a current density of 20 A g^{-1} and the results are shown in Fig. 6A. The capacitance decay over 2000 cycles is ~15%, indicating excellent long-term capacitive stability.

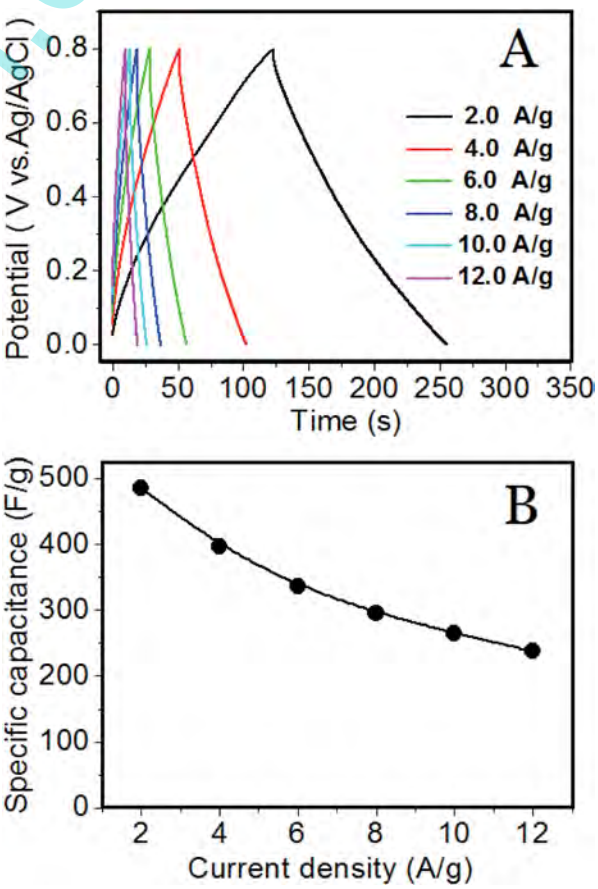

Fig. 5 (A) Charge–discharge curves at various current densities for MnO_2/ACP; (B) specific capacitance calculated based on charge–discharge curves from plot (A) as a function of current density.

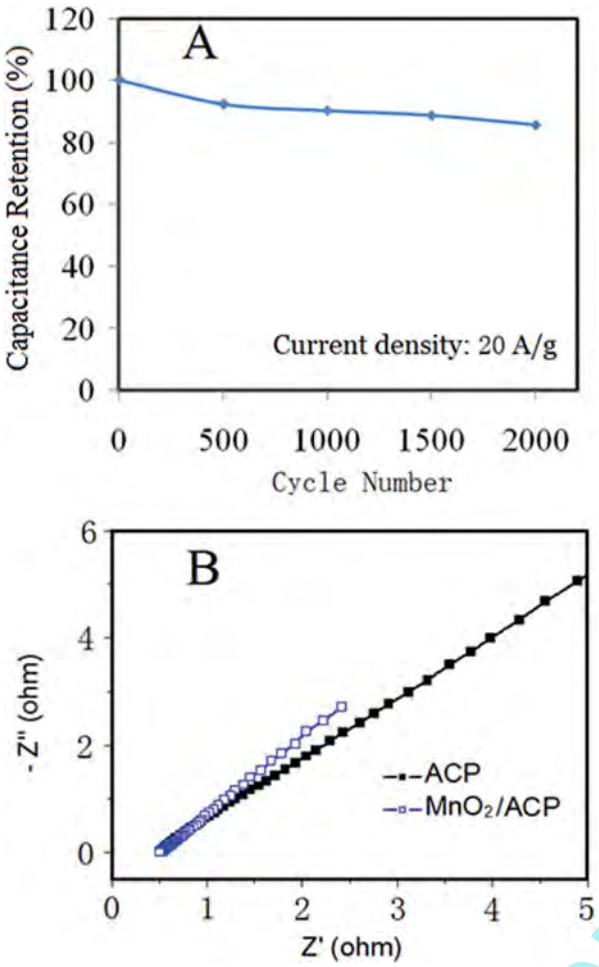

Fig. 6 (A) Capacitance retention test over 2000 cycles at a current density of 20 A g^{-1} for MnO_2/ACP; (B) Nyquist electrochemical impedance spectra for ACP and MnO_2/ACP.

To further study the resistance of the supercapacitor with the CP and ACP electrodes, electrochemical impedance spectroscopy (EIS) data were collected and are shown in Fig. 6B. The Nyquist-type impedance spectra for ACP and MnO_2/ACP electrodes shown in Fig. 6B contain only upward sloping lines, indicating that both electrodes have low diffusion resistance and exhibit good capacitive performance.[30,31]

In order to design high performance supercapacitors, several factors have to be considered. In our study, the electronic conductivity of the composited MnO_2/ACP and the electrochemical advantage of the MnO_2 material are important. First, considering that the electronic conductivity of MnO_2/ACP largely depends on the surface structure of ACP and the interaction between the MnO_2 film and ACP, the carbon paper was treated by the modified Hummers method to improve its hydrophilicity and to enhance its interaction with the deposited MnO_2. Second, a very thin MnO_2 film deposited on the ACP makes electrolytic ions easily access the active material, such that the full advantage of MnO_2 as electrode active material for supercapacitor can be realized. In brief, the electrodeposition of MnO_2 thin film on activated carbon paper (MnO_2/ACP) is reported for the first time, and the composited MnO_2/ACP is considered as a promising electrode material for building up efficient supercapacitors.

4. Conclusion

In summary, manganese dioxide (MnO_2) electrodeposited over activated carbon paper (ACP) to form a composite MnO_2/ACP material was prepared and characterized by the SEM, EDS, AFM, XRD and contact angle testing. Further, the supercapacitive behaviors of samples were measured by the cyclic voltammetry (CV) and galvanostatic charge–discharge. The as-prepared MnO_2/ACP shows excellent capacitance performance with a high specific capacitance of 485.4 F g^{-1} calculated from discharge curve with a current density of 2 A g^{-1}, owing to its enlarged specific surface area and improved electronic conductivity. Moreover, the specific capacitances of MnO_2/ACP obtained from cyclic voltammograms at scan rates of 20 and 50 mV s^{-1} are 312.0 and 235.2 F g^{-1}, which retain 81.7% and 61.6% of the corresponding value at 10 mV s^{-1} (382.0 F g^{-1}). This indicates that MnO_2/ACP possesses better rate capability as active electrode material for supercapacitors compared to others due to the easy access of electrolytic ions, leading to the full utilization of MnO_2 active material for supercapacitors. To summarize, the electrodeposition of MnO_2 thin film on activated carbon paper (MnO_2/ACP) is reported for the first time, and the composite MnO_2/ACP is a promising electrode material for building up efficient supercapacitor.

Acknowledgements

The work described in this paper was supported by the National Natural Science Foundation of China (no. 51206029)

Notes and references

1 P. Simon and Y. Gogotsi, *Nat. Mater.*, 2000, **91**, 845–854.
2 A. Burke, *J. Power Sources*, 2000, **91**, 37–50.
3 J. P. Zheng, P. J. Cygan and T. R. Jow, *J. Electrochem. Soc.*, 1995, **142**, 2699–2703.
4 M. H. Yu, T. Zhai, X. H. Lu, X. J. Chen, S. L. Xie, W. Li, C. L. Liang, W. X. Zhao, L. P. Zhang and Y. X. Tong, *J. Power Sources*, 2014, **239**, 64–71.
5 S. C. Pang, M. A. Anderson and T. W. Chapman, *J. Electrochem. Soc.*, 2000, **147**, 444–450.
6 H. M. Lee, K. T. Lee and C. K. Kim, *Materials*, 2014, **7**, 265–274.
7 S. J. He, C. X. Hu, H. Q. Hou and W. Chen, *J. Power Sources*, 2014, **246**, 754–761.
8 Z. B. Lei, J. T. Zhang and X. S. Zhao, *J. Mater. Chem.*, 2012, **22**, 153–160.
9 S. W. Lee, J. Kim, S. Chen, P. T. Hammond and Y. Shao-Horn, *ACS Nano*, 2010, **4**, 3889–3896.
10 F. Cao, Y. M. Liu, B. L. Chen, L. F. Fei, Y. Wang and J. K. Yuan, *Electrochim. Acta*, 2012, **81**, 1–7.
11 G. P. Xiong, K. P. S. S. Hembram, R. G. Reifenberger and T. S. Fisher, *J. Power Sources*, 2013, **227**, 254–259.

12 X. Zhao, L. L. Zhang, S. Murali, M. D. Stoller, Q. H. Zhang, Y. W. Zhu and R. S. Ruoff, *ACS Nano*, 2012, **6**, 5404–5412.
13 B. G. Choi, Y. S. Huh, W. H. Hong, H. J. Kim and H. S. Park, *Nanoscale*, 2012, **4**, 5394–5400.
14 D. Y. Zhai, B. H. Li, H. D. Du, G. Y. Gao, L. Gan, Y. B. He, Q. H. Yang and F. Y. Kang, *Carbon*, 2012, **50**, 5034–5043.
15 D. K. Walanda, G. A. Lawrance and S. W. Donne, *J. Power Sources*, 2005, **139**, 325–341.
16 M. H. Chakrabarti, N. P. Brandon, S. A. Hajimolana, F. Tariq, V. Yufit, M. A. Hashim, M. A. Hussain, C. T. J. Low and P. V. Aravind, *J. Power Sources*, 2014, **253**, 150–166.
17 B. Sun and M. Skyllas-Kazacos, *Electrochim. Acta*, 1992, **37**, 1253–1260.
18 L. Yue, W. Li, F. Sun, L. Zhao and L. Xing, *Carbon*, 2010, **48**, 3079–3090.
19 X. X. Wu, H. F. Xu, P. C. Xu, Y. Shen, L. Lu, J. C. Shi, J. Fu and H. Zhao, *J. Power Sources*, 2014, **263**, 104–109.
20 W. S. Hummer and R. E. Offeman, *J. Am. Chem. Soc.*, 1958, **80**, 1339.
21 J. Yan, Z. J. Fan, T. Wei, J. Cheng, B. Shao, K. Wang, L. P. Song and M. L. Zhang, *J. Power Sources*, 2009, **194**, 1202–1207.
22 O. Durupthy, J. Bill and F. Aldinger, *Cryst. Growth Des.*, 2007, **7**, 2696–2704.
23 T. S. Chow, *J. Phys.: Condens. Matter*, 1998, **10**, L445–L451.
24 N. Giovambattista, P. G. Debenedetti and P. J. Rossky, *J. Phys. Chem. B*, 2007, **111**, 9581–9587.
25 Y. Shi, L. J. Pan, B. R. Liu, Y. Q. Wang, Y. Cui, Z. A. Bao and G. H. Yu, *J. Mater. Chem. A*, 2014, **2**, 6086–6091.
26 F. Yang, J. Y. Yao, F. L. Liu, H. C. He, M. Zhou, P. Xiao and Y. H. Zhang, *J. Mater. Chem. A*, 2013, **1**(3), 594–601.
27 S. M. Zhu, H. S. Zhou, M. Hibino, I. Honma and M. Ichinara, *Adv. Funct. Mater.*, 2005, **15**, 381–386.
28 R. K. Sharma, H. S. Oh, Y. G. Shul and H. Kim, *Phys. B*, 2008, **403**, 1763–1769.
29 Y. C. Qiu, Y. H. Zhao, X. W. Yang, W. F. Li, Z. H. Wei, J. W. Xiao, S. F. Leung, Q. F. Lin, H. K. Wu, Y. G. Zhang, Z. Y. Fan and S. H. Yang, *Nanoscale*, 2014, **6**, 3626–3631.
30 C. W. Huang, C. A. Wu and S. S. Hou, *Adv. Funct. Mater.*, 2012, **22**, 4677–4685.
31 Z. Gui, H. L. Zhu and E. Gillette, *ACS Nano*, 2013, **7**, 6037–6046.